AIP | The Journal of Chemical Physics

Communication: Dominance of extreme statistics in a prototype many-body Brownian ratchet

Evan Hohlfeld and Phillip L. Geissler

Citation: The Journal of Chemical Physics **141**, 161101 (2014); doi: 10.1063/1.4899052
View online: http://dx.doi.org/10.1063/1.4899052
View Table of Contents: http://scitation.aip.org/content/aip/journal/jcp/141/16?ver=pdfcov
Published by the AIP Publishing

Communication: Dominance of extreme statistics in a prototype many-body Brownian ratchet

Evan Hohlfeld[1,a)] and Phillip L. Geissler[1,2,b)]
[1]*Lawrence Berkeley National Laboratory, Berkeley, California 94720, USA*
[2]*Department of Chemistry, University of California, Berkeley, California 94720, USA*

(Received 20 August 2014; accepted 10 October 2014; published online 27 October 2014)

Many forms of cell motility rely on Brownian ratchet mechanisms that involve multiple stochastic processes. We present a computational and theoretical study of the nonequilibrium statistical dynamics of such a many-body ratchet, in the specific form of a growing polymer gel that pushes a diffusing obstacle. We find that oft-neglected correlations among constituent filaments impact steady-state kinetics and significantly deplete the gel's density within molecular distances of its leading edge. These behaviors are captured quantitatively by a self-consistent theory for extreme fluctuations in filaments' spatial distribution. © *2014 AIP Publishing LLC*. [http://dx.doi.org/10.1063/1.4899052]

Living systems have evolved many processes that exploit fluctuations at the sub-cellular scale to transmute chemical energy into mechanical work. These processes, collectively referred to as Brownian ratchets, propel cell motions such as crawling, phagocytosis, and chromosome separation during anaphase.[1] They generally operate by an irreversible discrete chemical process stochastically ratcheting the advance of a continuously diffusing degree of freedom. For example, the essentially irreversible polymerization of an actin filament can lock in the diffusive advance of a load-bearing obstacle[2] such as the cell membrane, a synthetic microbread,[3,4] or an atomic force microscope cantilever.[5]

Two-body Brownian ratchets, in which rectification is driven by a single stochastic process, have been analyzed extensively. In particular, the basic problem of a single polymerizing filament growing against a diffusive barrier under load has been solved exactly.[2] These model problems have been widely used to discuss and rationalize the behavior of many-body systems that are less tractable but more directly relevant to biological motility (e.g., a collection of polymerizing filaments that push on a diffusing obstacle).[6–14] To do so, extant theories (and many simulations as well) have appealed to approximations that are not generally justified by the underlying chemical kinetics. For example, it is commonly assumed that nonequilibrium considerations are important only for the discrete, driven part of the ratcheting process; all other degrees of freedom are imagined to follow adiabatically. In this approximation, the fluctuating obstacle is replaced by an effective, steady force acting directly on the discrete elements of the ratchet. This assumption of rapid equilibration is explicit in some stochastic models of polymerization ratchets,[6–10] implicit in some phenomenological models of actin gels,[11,12] and inherent to continuum models of growing gels.[13,14] While this effective-force approximation can be justified on thermodynamic grounds when external loads are sufficiently strong to stall the ratchet,[8] most biological ratchets operate far from stall conditions.

In this Communication, we develop a different theory of a model N-filament polymerization ratchet (see Fig. 1), one that embraces many-body correlations in a fully nonequilibrium dynamics. Our analysis shows that the influence on a given filament's growth due to the ratcheting action of its peers does not obey a simple law of large numbers. Specifically, a mean field theory which neglects correlated fluctuations in the positions of different filaments does not agree with exact numerical simulations. The surprisingly influential correlations neglected by mean field theory emerge from the nonequilibrium nature of obstacle motion, and we find they can be captured by a self-consistent theory for extreme fluctuations within the polymerizing gel. In effect, this theory recognizes that the diffusing obstacle interacts only with the instantaneously leading filament, an extreme member of the filament distribution. By factorizing a two-point correlation function involving the lead filament, we derive an effective equation of motion that very successfully captures the structure and kinetics of the prototype model. The form of this theory, as well as its basic predictions, should be straightforward to generalize for other many-body ratchets.

The specific model we study, sketched in Fig. 1, is a generalization of the $N = 1$ ratchet[2] to the multi-filament case. Like that model ours focuses on the generic physical features that are essential to its function. In detail, we consider N parallel, straight, rigid filaments (comprising the "gel") that push, via polymerization, against a diffusing obstacle with diffusion constant D and no external load. The position x_i of filament tip i advances stochastically in the $+x$ direction as a conditional Poisson process, taking discrete, irreversible steps of size a with mean rate k_{on} so long as monomer addition would not penetrate the obstacle at position y. The obstacle in turn diffuses freely with a reflecting boundary condition at the leading edge of the gel, $X \equiv \max_i x_i$. Our explicit treatment of the obstacle allows us to study the nonequilibrium correlations inherent in the ratchet.

a)Electronic mail: evanhohlfeld@gmail.com
b)Electronic mail: geissler@berkeley.edu

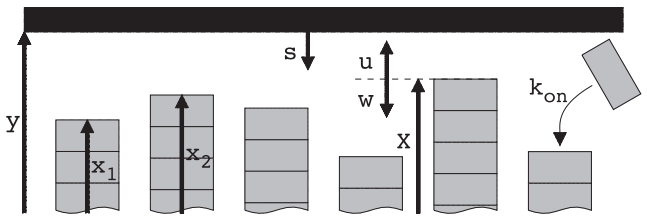

FIG. 1. Monomers (gray rectangles) stochastically polymerize onto existing filaments with heights x_i, while the obstacle (thick black line) at y executes unbiased, one dimensional diffusion. The coordinate s is measured relative to y. Coordinates u and w are measured relative to $X \equiv \max[\{x_i\}_{i=1}^{N}]$.

We imagine that the base of each filament is firmly anchored (as in the $N = 1$ model), so that x_i increases in time on a fixed one-dimensional lattice. Because the actin gels we have in mind are highly disordered materials, we take the offsets among these lattices to be randomly distributed.[18] Adopting units of length and time such that $a = 1$ and $k_{on} = 1$, the number of filaments N and the diffusion constant D (measured in units of $k_{on}a^2$) are the only dimensionless parameters in our model. Biological values of this dimensionless diffusivity in actin-based systems range broadly, from $D = 10$ for an actin filament pushing a patch of cell membrane[16] to $D = 10^{-2}$ for a similar actin filament pushing the bacterium *L. monocytogenese* through viscous cytoplasm.[6]

We generated stochastic trajectories of our model using the continuous time Monte Carlo (CTMC) method, which samples ratcheting dynamics efficiently and exactly. Our implementation of CTMC is detailed in the supplementary material.[15]

Our key numerical results include the drift velocity v, the spatially resolved average density of filament tips, and statistics of the lead filament's distance from the obstacle. The small-N and large-N limits of v are dictated, respectively, by the exact solution for $N = 1$[2] and the average unobstructed polymerization velocity $v = 1$ as $N \to \infty$. Our simulation results presented in Fig. 2 show that the crossover between

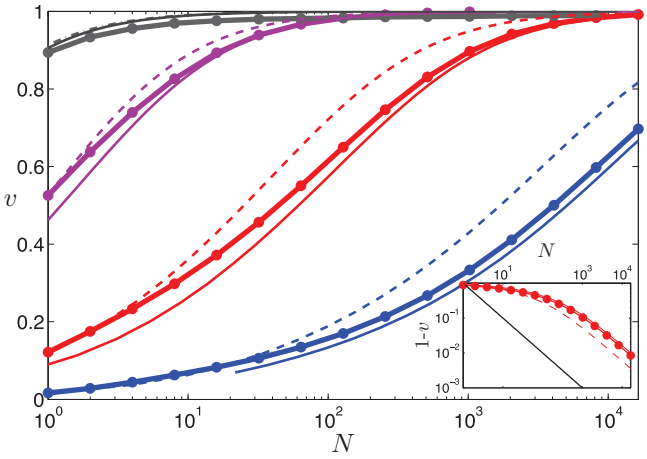

FIG. 2. Steady-state drift velocity v as a function of the number N of pushing filaments. Results are shown for simulations [points (•) with thick solid lines to guide the eye] and predictions from MF theory (dashed lines) and from XF theory (solid lines). Colors indicate different obstacle mobilities: $D = 10$ (black), 1 (magenta), 0.1 (red), and 0.01 (blue). (Inset) $1 - v(N)$ (colors and markers as in the main panel) compared with $1/N$ (solid black line).

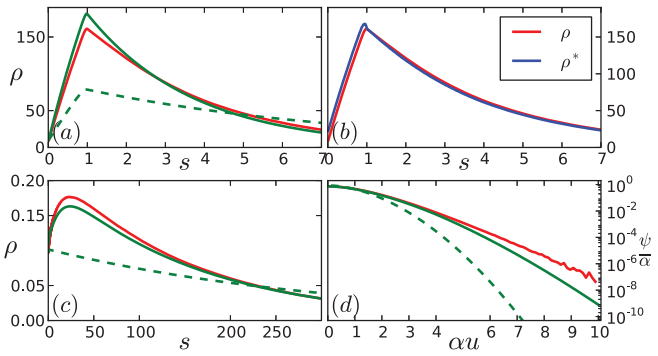

FIG. 3. Steady-state gel structure as determined from simulation and theory. In (a), (b), and (d) $D = 0.1$ and $N = 600$. (a) Filament tip density $\rho(s)$, from simulation (red line), from MF theory (dashed green line), and from XF theory (solid green line). (b) $\rho(s)$ (red line) and $\rho^\star(s)$ (blue line), both from simulation. (c) $\rho(s)$ for $D = 10$ and $N = 32$ from simulation (red), MF theory (dashed green line), and XF theory (solid green line). (d) Scaled distribution $\psi(u)$ of the extreme statistic $u = y - X$ from simulation (red), from MF theory (dashed green line), and from XF theory (solid green line). The scaling parameter $\alpha = [\eta(1)/D]^{1/3} \approx 10$.

these limits is gradual, with $v \sim \log N$ over a large, intermediate range of N. For $N \gg 1$ we find that $v \approx 1 - \xi(D)/N$, where $\xi(D)$ is a dimensionless function of D.

As we show in Figs. 3(a) and 3(d), for $N > 1$ the linear density of filament tips at distance s from the obstacle, $\rho(s)$, is marked by a molecular-scale layer of depleted filament density adjacent to the obstacle. In the case of low obstacle mobility, the filament density can vary by many orders of magnitude just within a single monomer distance away from the obstacle. Suggestively, a depleted layer of similar structure appears in the tip distribution function of a low-mobility $N = 1$ ratchet when subjected to an external propulsive force. We will show that accurately capturing this non-monotonic density profile requires a theory that carefully addresses extreme fluctuations in filament density.

To clarify the relationship between steady state kinetics and microscopic structure at the gel's leading edge, we develop approximate analytical solutions to the master equation for the time-dependent configurational probability $P(t, y, x_1, \ldots, x_N)$ of our N-filament model,[19]

$$P_t = DP_{yy} + \sum_{i=1}^{N}[P(t, y, \ldots, x_i - 1, \ldots) - P\Theta(y - x_i - 1)] \quad (1)$$

[coordinate-name subscripts (i.e., t and y, and later s and u) denote partial derivatives]. The first term on the right-hand side of Eq. (1) represents free diffusion of the obstacle. The remaining terms, which involve the shifted coordinates $x_i \to x_i - 1$ and the Heaviside function $\Theta(x)$, represent stochastic growth of the filaments as constrained by the obstacle. Because obstacle diffusion is a continuous process, the mutual impenetrability of the obstacle and gel requires the boundary condition $P_y(\{y = x_i\}) = 0$ to prevent flux of probability to configurations that violate constraints of volume exclusion. For $N = 1$, Eq. (1) is identical to the equation of motion studied in Ref. 2.

We derive several exact relationships by evaluating moments of Eq. (1) (detailed calculations appear in the supplementary material[15]). In particular, at steady state the average y-current ($\int y P_t\, dx^N dy$) yields the mean drift velocity v. Integrating by parts over y, we can write this moment in terms of average structural properties, specifically the filament tip density $\rho(s) \equiv \int_{\{x_i<y\}} \sum_i \delta(s-y+x_i) P\, dx^N dy$ at a distance s from the obstacle [where $\delta(x)$ is the Dirac δ-function]:

$$v = D\rho(0). \tag{2}$$

According to this relation, the effective force exerted on the obstacle, v/D, is proportional to the average number of filaments *in contact* with it, which is strongly shaped by multi-filament correlations.

We derive an exact equation for $\rho(s)$ from Eq. (1) by multiplying both sides by the density operator $\sum_i \delta(s-y+x_i)$ and integrating over $x_1, \ldots, x_N$,

$$D\rho_{ss} - D\rho_s^{(2)}(0,s) + \rho(s+1) - \rho\Theta(s-1) = 0. \tag{3}$$

The corresponding boundary condition, $\rho_s(0) = \rho^{(2)}(0,0)$, can be obtained in similar fashion. These results involve, but do not determine, the two-point correlation function $\rho^{(2)}(s,s') \equiv \int_{\{x_i<y\}} \sum_{i\neq j} \delta(s-y+x_i)\delta(s'-y+x_j) P\, dx^N dy$.

The steady state equation (3) differs from a single-filament master equation only through the term $D\rho_s^{(2)}(0,s)$, which describes a current of filament density induced by many-body effects. Its form resembles the contribution $DF\rho_s(s)$ that would arise from a constant, propulsive external force F. This similarity suggests conceiving the many-filament ratchet in terms of a single tagged filament pushing an obstacle that additionally experiences a fluctuating force due to the remaining $N-1$ filaments. The challenge from this perspective lies in addressing correlations between the tagged filament's progress and fluctuations in the effective driving force. One might naturally expect that such fluctuations become less important with increasing N and are ultimately irrelevant in the limit $N \to \infty$. This notion motivates a mean-field (MF) approximation to Eq. (3), which posits a factorization of the two-point function, $\rho^{(2)}(s,s') = \frac{N-1}{N}\rho(s)\rho(s')$, and thus neglects correlated fluctuations in the growth of distinct filaments. [The coefficient $(N-1)/N$ ensures proper normalization of $\rho^{(2)}$.] Figure 3(b) assesses the MF ansatz by comparing simulation results for $\rho^\star(s) \equiv [N/(N-1)]\rho^{(2)}(0,s)/\rho(0)$ and $\rho(s)$. These functions are indeed almost indistinguishable by eye.

The mean field factorization renders Eq. (3) simple both to solve and to interpret. It describes a single stochastically growing filament and an obstacle that diffuses under a constant pulling force $\mathcal{F} = \frac{N-1}{N}\rho(0)$. The strength of this force (which represents ratcheting by the remainder of the gel) must be determined self-consistently, through the nonlinear boundary condition $\rho_s(0) = \mathcal{F}\rho(0)$. The exact solution for this effective one-dimensional system recapitulates some of the qualitative behaviors revealed by our simulations.

In particular, MF theory captures the emergence of a depletion layer [i.e., large and positive density gradient $\rho_s(0)$] for small D, which can be viewed as a straightforward consequence of flux balance. When $s > 1$, the tagged filament can polymerize freely. For low obstacle mobility, the corresponding contributions to Eq. (3) (the latter two terms on the right-hand side) nearly balance, describing steady flux of filament tip density towards the obstacle [and consequent steady increase in $\rho(s)$ as s decreases]. In $s < 1$ the tagged filament stalls; the influx $\rho(s+1)$ of polymerizing filaments in Eq. (3) must be balanced instead by the MF drift $D\mathcal{F}\rho_s$. As $\rho(1)$ is large, due to the flux from $s > 1$,[20] so must be $\rho_s(0)$.

Given the close agreement between $\rho^\star(s)$ and $\rho(s)$ in Fig. 3(b), predictions of MF theory for the relationship between N and v are surprisingly inaccurate (see Fig. 2). In particular, the number of filaments required to sustain an average speed of $v \approx 1/2$ errs by more than a factor of two for the lowest obstacle mobilities we have simulated. More troublingly, this error persists for large N and appears to grow as D decreases, i.e., as the number of contacting filaments, $\rho(0) \sim v/D$, *increases* [see Eq. (2)] and precisely where the MF approximation seems best justified. Furthermore, MF theory misses qualitative features of ρ when D is large, most notably the persistence of the depleted layer even for $D \gg 1$ (see Fig. 3(c)). The inter-filament correlations neglected in MF theory, while small in absolute magnitude, are thus highly influential for kinetics, especially in the limit $N \to \infty$.

The failure of MF theory motivates a shift in perspective and strategy, away from characterizing the *average* behavior of a filament and towards understanding statistics of the gel's leading edge. After all, the obstacle is obstructed at any moment only by the one filament that has grown the farthest. We therefore focus on the distance $u = y - X$ between the obstacle and lead filament, whose statistical distribution $\psi(u) \equiv \int \delta(u-y+X) P\, dx^N dy$ also directly determines steady state kinetics: $v = D\psi(0)$ (see the supplementary material[15]). Our theory for the extreme fluctuations characterized by $\psi(u)$ begins with an exact but incomplete relation:

$$D\psi_{uu} = \int_0^1 [\Pi(u,w)\Theta(w+u-1) - \Pi(u-w+1,w)]dw, \tag{4}$$

together with the boundary condition $\psi_u(0) = 0$. In Eq. (4), the joint probability $\Pi(u,w) \equiv \int \sum_{j=1}^N \delta(u-y+X)\delta(w-X+x_j) P\, dx^N dy$ characterizes correlations between the position of the lead filament and filament density fluctuations at a lag distance w behind the lead filament (see coordinate definitions in Fig. 1). Because distances in the X-based and y-based coordinate systems are related by the equation $u + w = s$, we can derive exact relationships between Π, ρ, and $\rho^{(2)}$ which clarify the relationship between the lead- and average-filament centered descriptions of filament density:

$$\rho(s) = \int_0^s \Pi(u, s-u)\, du, \tag{5a}$$

$$\rho^{(2)}(0,s) = \lim_{\epsilon\to 0^+} \Pi(0, s+\epsilon). \tag{5b}$$

We construct a closed set of equations through an approximate factorization (denoted by over bars),

$$\bar{\Pi}(u,w) = \bar{\psi}(u)\bar{\sigma}(w), \tag{6}$$

in which the filament density $\sigma(w) \equiv \int \sum_{j=1}^{N} \delta(w - X + x_j) P\, dx^N dy$ is resolved relative to the lead filament position. Since one filament resides at $w = 0$ by definition, $\sigma(w)$ contains a singular part that is conveniently separated from a meaningful measure of the gel's internal structure, $\eta(w) = \sigma(w) - \delta(w)$. We will refer to the theory based on (6) as extreme field (XF) theory. The solution of XF theory for $N \gg 1$ agrees very closely with CTMC simulations, see the supplementary material[15] and Figs. 2, 3(a), 3(c), and 3(d).

The equations of XF theory describe fluctuations of a tagged filament [whose distance s from the obstacle is distributed according to $\bar{\rho}(s)/N$] interacting with an obstacle that is driven by another filament [notionally the lead filament, whose separation u from the obstacle is independently distributed as $\bar{\psi}(u)$]. Since $\bar{\rho}$ and $\bar{\psi}$ are different statistics of the same population, they are coupled by the self-consistency condition [Eqs. (5a) and (6)]:

$$\bar{\rho}(s) = \bar{\psi}(s) + \int_0^s \bar{\psi}(u)\bar{\eta}(s-u)\, du. \tag{7}$$

In MF theory, the obstacle that impedes growth of a tagged filament is driven by a constant force representing the rest of the gel; beyond the steady propulsion, many-body contributions do not change the character of this effective obstacle's motion. Nonequilibrium dynamics of such an effective obstacle are treated very differently in XF theory. The distinction is most apparent in the limit that $D \gg 1$ and $N \gg 1$. Here, XF theory predicts a simple gel structure, with filament tip density decaying exponentially behind the lead filament, $\bar{\eta}(w) \sim D^{-1} \exp[(v-1)w]$. The corresponding sparseness of the gel in the vicinity of the obstacle implies that $\bar{\psi}$ differs little from its $N = 1$ form, just as observed in simulations. These results for η and ψ, together with the self-consistency imposed by Eq. (7), yield a zone of depleted filament density over a length scale $\sim D$, again in close agreement with simulation. In this analysis depletion arises in the large-D limit from large excursions of the obstacle away from the gel's leading edge, an effect that cannot be captured by MF theory. For the case of actin and mobility $D \sim 10$, these excursions occur on a length scale of order ten nanometers, which in principle could be resolved experimentally using fluorescence resonance energy transfer techniques.

XF and MF theories also differ in their predictions for gel structure far from the leading edge, $s \gg D$. In this region we can solve Eqs. (7), (5b), and (6) for $\rho^{(2)}(0, s)$ in terms of the gradients of ρ,

$$\bar{\rho}^{(2)}(0, s) \sim \bar{\rho}(0)\bar{\rho} + \chi \bar{\rho}_s + \cdots, \tag{8}$$

where $\chi \equiv \bar{\psi}(0) \int_0^\infty u\bar{\psi}(u)\, du$. Substituting Eq. (8) into (3) yields an equation similar to the MF equation for ρ:

$$D_{\text{ren}}\bar{\rho}_{ss} - v\bar{\rho}_s(s) + \bar{\rho}(s+1) - \bar{\rho}\Theta(s-1) = 0, \tag{9}$$

where the renormalized diffusivity $D_{\text{ren}} = (1 - \chi)D$ ranges from $\lim_{D \to 0} D_{\text{ren}}/D = 0.3156$ to $\lim_{D \to \infty} D_{\text{ren}} = \frac{1}{2}$ (see the supplementary material[15]). The similarity of these asymptotes to the long-time diffusivity of the obstacle in an $N = 1$ ratchet (see the supplementary material[15]) suggests a simple physical understanding of mobility renormalization: From the perspective of a tagged filament far from the leading edge, the apparent random walk executed by the obstacle is not simply characterized by the bare mobility D, but is instead the result of independent ratcheting by the lead filament, which both induces drift and significantly suppresses fluctuations in the obstacle's motion.

As $D \to 0$, Eq. (9) becomes valid for all s (see the supplementary material[15]). Because this result embodies the self-consistent hypothesis of MF theory, we judge the role of extreme value statistics for small D to be less critical qualitatively than in the limit of high mobility. Quantitative agreement with simulations, however, is much improved even here by the XF renormalization of D. Furthermore, assuming filament heights to be independently distributed (as suggested by the MF ansatz) yields for small D a Gaussian form for ψ (see the supplementary material[15]), which does not match the compressed exponential decay that is obtained from simulations and is correctly predicted by XF theory (see Fig. 3(d)).

The fundamental shortcoming of MF theory for our model ratchet is the implicit assertion that many-body growth mechanisms can be compactly described in terms of the average behavior of individual filaments. By contrast, XF theory recognizes that constraints imposed by the obstacle select a sub-population of all fluctuating degrees of freedom for special treatment (i.e., the lead filament and obstacle). We expect that a similar focus on appropriate extreme statistics may be helpful in more complex models where biochemical processes at the obstacle-gel interface (e.g., filament branching in an autocatalytic gel[4,17]) further distinguish certain extreme filaments. The robust and as-yet-unobserved prediction of our theory and CTMC simulations that many-body correlations effect a precipitous drop in filament density within a molecular distance of the gel's leading edge certainly has significant implications for the dynamical consequences of these processes. In particular, we anticipate an augmentation of forces sustained by leading filaments, alteration of the transient binding between filaments and the obstacle during branching, and amplification of leading-edge fluctuations. These fundamentally non-continuum effects might be mimicked in continuum models of actin gels through a suitable choice of boundary conditions, providing a schematic assessment of their influences on scales inaccessible to microscopically detailed approaches.

We thank Dan Fletcher for stimulating discussions. This work was supported by the U.S. Department of Energy, Office of Basic Energy Sciences, Division of Materials Sciences and Engineering, under Contract No. DE-ACO2-05CH11231.

[1] D. Bray, *Cell Movements: From Molecules to Motility*, 2nd ed. (Garland Publishing, New York, 2001).
[2] C. S. Peskin, G. M. Odell, and G. F. Oster, Biophys. J. **65**, 316 (1993).
[3] L. A. Cameron, M. J. Footer, A. van Oudenaarden, and J. A. Theriot, Proc. Natl. Acad. Sci. U.S.A. **96**, 4908 (1999).
[4] S. Wiesner *et al.*, J. Cell Biol. **160**, 387 (2003).
[5] S. H. Parekh, O. Chaudguri, J. A. Theriot, and D. A. Fletcher, Nat. Cell Biol. **7**, 1219 (2005).
[6] A. Mogilner and G. Oster, Biophys. J. **71**, 3030 (1996).
[7] A. Mogilner and G. Oster, Biophys. J. **84**, 1591 (2003).
[8] J. Kierfeld and R. Lipowsky, Europhys. Lett. **62**, 285–291 (2003).
[9] T. E. Schaus and G. G. Borisy, Biophys. J. **95**, 1393 (2008).

[10]J. Krawczyk and J. Kierfeld, Europhys. Lett. **93**, 28006 (2011).
[11]A. E. Carlsson, Biophys. J. **84**, 2907 (2003).
[12]J. Weichsel and U. S. Schwarz, Proc. Natl. Acad. Sci. U.S.A. **107**, 6304 (2010).
[13]J. Plastino and C. Sykes, Curr. Opin. Cell Biol. **17**, 62 (2005).
[14]K. Sekimoto, J. Prost, F. Jülicher, H. Boukellal, and A. Bernheim-Grosswasser, Eur. Phys. J. E **13**, 247 (2004).
[15]See supplementary material at http://dx.doi.org/10.1063/1.4899052 for detailed calculations and discussion of numerical techniques.
[16]N. J. Burroughs and D. Marenduzzo, J. Chem. Phys. **123**, 174908 (2005).
[17]T. D. Pollard and G. G. Borisy, Cell **112**, 453 (2003).
[18]Setting the base of each filament at the same height, so that all filament sub-lattices lie in register, results in qualitatively different kinetics. For instance, the steady drift velocity v determined from simulations grows as N increases but saturates well below its kinetic limit of $k_{on}a$.
[19]Note that P describes an *ensemble* of N-filament ratchets with *uniformly distributed* lattice alignments. For small N, the dynamics depends strongly on the relative alignment of filaments; our approach averages over these alignments.
[20]Using the balance $D\mathcal{F}\rho_s(0) \sim \rho(1)$ with the MF boundary condition $\rho_s(0) = \mathcal{F}\rho(0)$ and the velocity relation $v = D\rho(0) \approx D\mathcal{F}$, we compute $\rho(1) \sim D\mathcal{F}^2\rho(0) \sim D^{-2}v^3$, which is large when $D \ll v^{3/2}$.